Analysis of Comodulation Effect Induced by Transmitting and Receiving Antennas and Correction Method in Bistatic SAR Radiometric Calibration

Qiaona Zheng, Yu Wang, *Member, IEEE*, Jun Hong, Feng Gao, and Shaoyan Du

***Abstract*— In the bistatic synthetic aperture radar (SAR), the comodulation effect induced by transmitting and receiving antennas to the image amplitude is the main factor affecting the radiometric accuracy. Therefore, the corresponding mechanism must be determined, and a correction method must be developed. However, there is no effective calibration target and method for measuring the bistatic SAR range round trip antenna pattern. In this letter, it is pointed out that the comodulation effect is not only related to the transmitting and receiving one-way antenna patterns but also to the range variation of the bistatic angle in the swath caused by the bistatic SAR observation geometry. To increase the radiometric accuracy in bistatic SAR images, a comodulation effect correction method based on accurate antenna models is proposed, and different error factors related to the range round trip antenna pattern are analyzed. Moreover, simulation experiments are conducted to verify the effectiveness of the proposed method.**

***Index Terms*— Bistatic synthetic aperture radar (SAR), comodulation effect, correction method, range round trip antenna pattern.**

I. Introduction

IN MONOSTATIC synthetic aperture radar (SAR), the modulation of the range (or elevation) round trip antenna pattern to the SAR image amplitude is the main factor affecting the radiometric accuracy, and this issue must be corrected in radiometric calibration [1]. Similarly, the comodulation effect induced by transmitting and receiving antennas is the main factor in bistatic SAR. For the monostatic SAR system, the range round trip antenna pattern can be directly measured by point target calibrators or distributed targets [2], [3], and the SAR image can be corrected using this antenna pattern. For the bistatic SAR system, since there is a lack of available point target calibrators and a few studies have focused on the bistatic scattering characteristics of distributed targets [4], [5], there are nearly no measurement methods for bistatic SAR range round trip antenna pattern. Theoretically, the transmitting and receiving one-way antenna patterns can be measured, respectively, by using ground transmitter or receiver [6], [7], but the comodulation still needs to be considered for bistatic SAR radiometric calibration and correction.

For bistatic SAR, the measurement of the range round trip antenna pattern is significantly more complex, and a few specific measurement methods have been given in the published studies. Moreover, a technique that uses the transponder is applicable for measuring the antenna patterns of bistatic SAR [8]. However, the design of active calibration targets does not consider the range variation of the bistatic angle in the swath, which may lead to incorrect measurement results. In addition, modern SAR systems based on active phased-array antennas typically have over thousands of antenna beams, and the in-orbit measurement of all the antenna beams with transponders is time-consuming, laborious, and costly [9], [10].

In this letter, we show that the range variation of the bistatic angle in the swath will affect the range round trip antenna pattern, which can provide guidance suggestion for designing, pointing, and field deployment of bistatic radiometric calibration equipment. Furthermore, based on the transmitting and receiving antenna models, a comodulation effect correction method for different antenna beams is proposed, which can be quickly calculated and performed according to the bistatic SAR observation geometry. This correction method is also valid for airborne bistatic SAR, especially with large bistatic angles, thus effectively improving the radiometric calibration accuracy.

The rest of this letter is organized as follows. Section II analyzes the influence mechanism of transmitting and receiving antennas to the bistatic SAR image amplitude. The error factors for the comodulation effect are analyzed in Section III. Section IV provides the comodulation effect correction method and verifies the correction method through simulation experiments. The conclusions are given in Section V.

II. Comodulation of Transmitting and Receiving Antennas

The bistatic SAR radar equation can be written as [11]

$$P_R = \frac{P_T g_T G_T(\theta_T, \phi_T) g_R G_R(\theta_R, \phi_R) \lambda^2}{(4\pi)^3 R_T^2 R_R^2} \sigma \tag{1}$$

Manuscript received May 31, 2019; revised June 28, 2020; accepted September 22, 2020. Date of publication October 27, 2020; date of current version December 21, 2021. This work was supported in part by the National Natural Science Foundation of China under Grant 61771453 and in part by the Equipment Development Department pre-research fund under Grant 6140416010202. *(Corresponding author: Qiaona Zheng.)*

Qiaona Zheng and Feng Gao are with the Key Laboratory of Aerospace Information Application Technology, 54th Research Institute, China Electronics Technology Group Corporation, Shijiazhuang 050081, China (e-mail: zhengqiaona16@mails.ucas.ac.cn).

Yu Wang, Jun Hong, and Shaoyan Du are with the National Key Laboratory of Science and Technology on Microwave Imaging, Institute of Electronics, Chinese Academy of Sciences, Beijing 100190, China.

Digital Object Identifier 10.1109/LGRS.2020.3030244

where P_T is the transmitting power, P_R is the receiving power, g_T is the processing gains of the transmitter, $G_T(\theta_T, \phi_T)$ is the transmitting antenna pattern, g_R is the processing gains of the receiver, $G_R(\theta_R, \phi_R)$ is the receiving antenna pattern, λ is the radar wavelength, R_T is the slant range from the transmitting antenna to target, R_R is the slant range from the target to the receiving antenna, respectively, and σ is the bistatic radar cross section (RCS) of the target.

After receiving the echo signal, the image is generated by the quantization processor and imaging processor, (1) can be written as

$$P_R^I(R) = \frac{P_T g_T G_T(\theta_T, \varphi_T) g_R G_R(\theta_R, \varphi_R) G_e G_p \lambda^2 \tau_p f_s}{(4\pi)^3 L_s} \times \left(\frac{T_s f_p}{R_T^2 R_R^2}\right) \sigma + P_n \quad (2)$$

where G_e is the quantization processing gain, G_p is the imaging processing gain, τ_p is the pulsewidth, f_s is the range resolution, f_p is the azimuth resolution, T_s is the synthetic aperture time, L_s is the propagation and system loss within the system signal path, and P_n is the noise.

Since $T_s = \min((Y_T/V), (Y_R/V))$ depends on the antenna with a relatively short time for the comment irradiation area [12], where V is the velocity and Y_T and Y_R represent the transmitting antenna and receiving antenna azimuth beamwidth, respectively, the bistatic SAR radiometric calibration model can be divided into two categories [13]. One is the T_s is determined by the transmitting antenna

$$P_R^I(R) = \frac{P_T g_T G_T(\theta_T, \varphi_T) g_R G_R(\theta_R, \varphi_R) G_e G_p \lambda^3 \tau_p f_s f_p}{(4\pi)^3 L_s V D_T} \times \left(\frac{1}{R_T R_R^2}\right) \sigma + P_n \quad (3)$$

the other is the T_s is determined by the receiving antenna

$$P_R^I(R) = \frac{P_T g_T G_T(\theta_T, \varphi_T) g_R G_R(\theta_R, \varphi_R) G_e G_p \lambda^3 \tau_p f_s f_p}{(4\pi)^3 L_s V D_T} \times \left(\frac{1}{R_T^2 R_R}\right) \sigma + P_n. \quad (4)$$

According to (3) and (4), the two antenna gain terms, $G_T(\theta_T, \phi_T)$ and $G_R(\theta_R, \phi_R)$, corresponding to the transmit and receive antennas, are functions of the elevation and azimuth angle at which a given target is observed and are major sources of calibration uncertainty. The antenna patterns must be known very precisely and corrected in radiometric calibration.

To facilitate the following analysis, the one-way antenna pattern is expressed as [14]:

$$G(\theta, \phi) = \sin c\left(\frac{\pi \cdot D_A(\sin\phi - \sin\phi_0)}{\lambda}\right) \cdot \sin c\left(\frac{\pi \cdot D_A(\sin\phi - \sin\phi_0)}{\lambda}\right) \quad (5)$$

where D_A and D_R are the antenna length in azimuth and elevation, respectively, ϕ is the azimuth angle, θ is the elevation angle, and (θ_0, φ_0) is the antenna beam pointing.

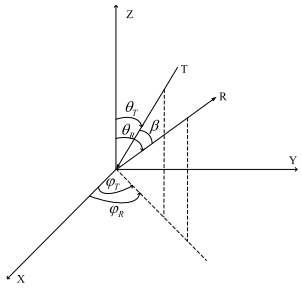

Fig. 1. Definition of azimuth and elevation angles.

The monostatic SAR uses a single location for both transmitter and receiver, so the round trip antenna pattern is $G^2(\theta, \varphi)$. However, the bistatic SAR operates with a separate transmitter and receiver. According to the bistatic SAR radar equation, the round trip antenna pattern can be expressed as follows:

$$F(\theta, \varphi) = G_T(\theta_T, \varphi_T) G_R(\theta_R, \varphi_R). \quad (6)$$

Due to the separation of the transmitter and receiver, the geometric configuration is more flexible, and the bistatic SAR imaging models are diversified, such as translation-invariant mode, constant velocity mode, and general mode. In addition, the bistatic SAR can be used in side- or forward-looking modes [15], [16]. In this letter, to maintain clarity and simplicity, the influence of the azimuth antenna pattern and the coupled effect with the range antenna pattern is not considered. We also assume that the bistatic SAR is working in side-looking translation-invariant mode. The elevation and azimuth angles of the round trip antenna pattern are based on the elevation and azimuth angles of the receiving antenna. As shown in Fig. 1, assuming that the target is located at the origin of the coordinates, (θ_T, φ_T) is the pointing angle of the transmitting beam to the target, and (θ_R, φ_R) is the pointing angle of the receiving beam to the target, where $\varphi_T = \varphi_R = \varphi$. Therefore, (6) can be written as

$$F(\theta_R, \varphi, \beta) = G_T(\theta_T, \varphi) G_R(\theta_R, \varphi). \quad (7)$$

The bistatic angle β is the angle between the transmitting beam and the receiving beam. According to Fig. 1, the bistatic angle satisfies $\beta = |\theta_T - \theta_R|$, so the round trip antenna pattern can be obtained by translation, as shown in Fig. 2.

However, according to the bistatic SAR observation geometry, the comodulation effect induced by the transmitting and receiving antennas is shown in Fig. 3. The gain and the corresponding product of the transmitting and receiving antenna pattern at different positions in the swath are calculated, and then, the range round trip antenna pattern can be obtained by interpolation. Taking the typical TanDEM-X satellite as an example [17], the system parameters are shown in Table I. The data in Fig. 4 show that the bistatic angle decreases gradually in the swath, indicating that the range variation of the bistatic angle should be considered when calculating the pattern antenna in a point-by-point approach. In practice, we should design or deploy the active or passive calibrators according to the variation of the bistatic angle, which could

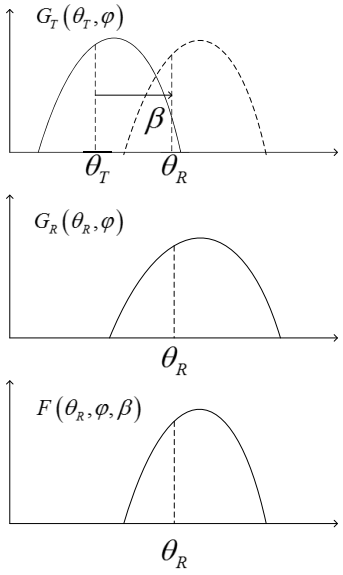

Fig. 2. Translation process.

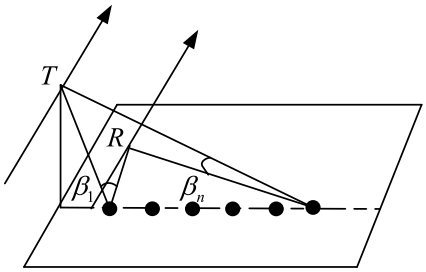

Fig. 3. Principle of the comodulation effect.

TABLE I
TANDEM-X SYSTEM PARAMETERS

Parameter	Value
Center Frequency	9.65 GHz (X-Band)
Chip Bandwidth	100 MHz
Satellite Height	511.5× 10^3 m
Antenna Length	4.8 m
Antenna Width	0.7 m
Antenna Mounting	33.8°
Cross-track Baseline	600 m

lead to difficulties in the measurement process. Therefore, this letter does not refer to the antenna pattern measurement equipment and method, and the antenna pattern synthesis is based on the transmitting and receiving antenna models.

III. Error Factors of the Comodulation Effect

This section presents an analysis of the error factors, focusing on the variation of the bistatic angle and the beam pointing error of the comodulation effect.

A. Variation of the Bistatic Angle

First, TanDEM-X is used as an example to analyze the variation of the bistatic angle for the range round trip antenna pattern as the bistatic SAR with a small bistatic angle. We can calculate that the bistatic angle corresponding to the center of

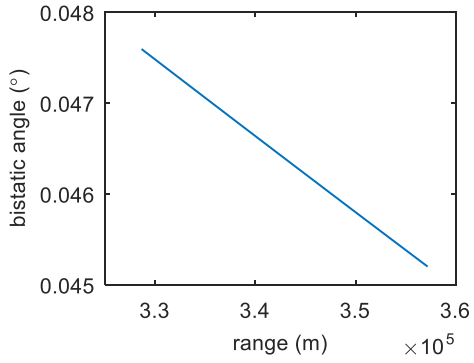

Fig. 4. Bistatic angle in different ranges.

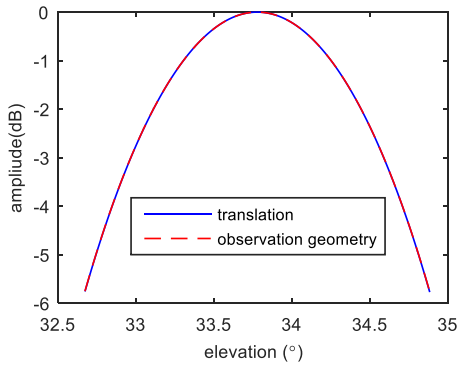

Fig. 5. Effect of the variation in the bistatic angle on the range round trip antenna pattern.

the width as 0.0464°. Fig. 5 shows the range round trip antenna patterns obtained by translating the bistatic angle corresponding to the center of the swath (Fig. 2) and performing point-by-point calculations based on the bistatic observation geometry (Fig. 3), respectively. Under the condition of a small bistatic angle, the maximum variation of bistatic angle in the swath is very small, approximately 0.002°, but this variation still leads to a difference in the range round trip antenna patterns obtained by the translation and observation geometry of less than 0.01 dB. Thus, whether the variation of the bistatic angle in different ranges is considered or not, the difference in the final range round trip antenna patterns will be very small.

For the bistatic SAR with a large bistatic angle, there are no eligible system parameters for satellite in orbit, so the system parameters from airborne bistatic SAR experiments performed by DLR and ONERA [18] are used to analyze the large bistatic angle case, as shown in Table II. The bistatic angle corresponding to the center of the width is 25.1506°, and the range round trip antenna pattern is shown in Fig. 6. As is pointed out, the bistatic angle decreases gradually in the swath, and the maximum variation is approximately 9° in this case. Furthermore, the difference in the range round trip antenna patterns obtained by translation and observation geometry is more than 0.5 dB, which cannot be neglected. Therefore, the variation of the bistatic angle in the swath is the main factor affecting the comodulation effect of the transmitting and receiving antennas, and thus, the accuracy of the range round trip antenna pattern can be guaranteed.

TABLE II
RAMSES AND E-SAR SYSTEM PARAMETERS

Parameter	Value
Center Frequency	9.6 GHz (X-Band)
E-SAR Flight Altitude	3198 m
RAMSES Flight Altitude	3048 m
E-SAR Elevation Beamwidth	35°
RAMSES Elevation Beamwidth	16°
E-SAR Boresight Angle	55°
RAMSES Boresight Angle	30°
Cross-track Baseline	2900 m

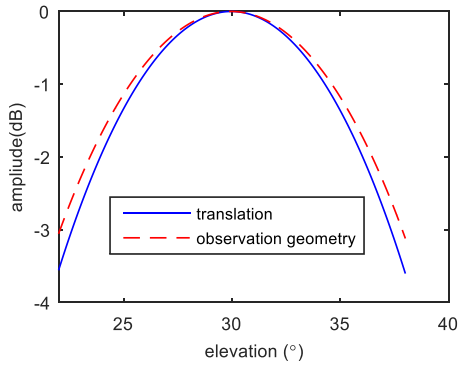

Fig. 6. Effect of the variation in the bistatic angle on the range round trip antenna pattern.

B. Beam Pointing Error

The beam pointing error in the elevation is mainly caused by mechanical and electrical antenna pointing issues and incorrect attitude (roll) control offsets. When the transmitting and receiving antennas have pointing deviations in opposite directions, the range overlap area will be greatly reduced, resulting in errors in the final range round trip antenna pattern. As the beam pointing error in elevation is 0.015° [19], we can calculate the effect of the beam pointing error for the range round trip antenna pattern. As shown in Fig. 7, a pointing error of 0.015° could introduce no more than a 0.16-dB antenna error, which indicates that for a general satellite pointing accuracy, the accuracy of the range round trip antenna pattern obtained based on the bistatic observation geometry is relatively high and can be used for correction. Therefore, the beam pointing error in the elevation must be controlled within a certain range according to the radiometric calibration accuracy.

IV. SIMULATION EXPERIMENTS OF THE COMODULATION EFFECT CORRECTION METHOD

We have analyzed the comodulation effect introduced by transmitting and receiving antennas and presented the comodulation effect principle and the range round trip antenna pattern in Section II, which can be used to correct the bistatic SAR image amplitude. Theoretically, the antenna pattern correction normalizes the pattern gain by multiplying the reciprocal of the range round trip antenna pattern by the radar data [1].

The main processing flow of antenna pattern correction is shown in Fig. 8 and described as follows.

1) Obtain the range round trip antenna pattern based on the bistatic observation geometry (see Fig. 3).

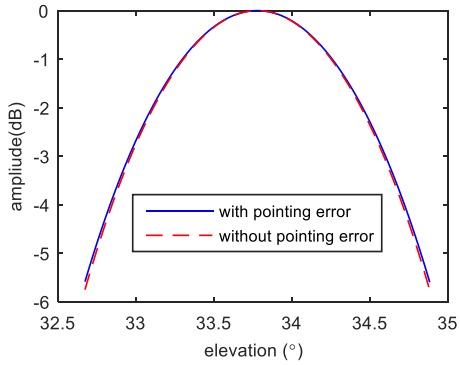

Fig. 7. Effect of the beam pointing error on the range round trip antenna pattern.

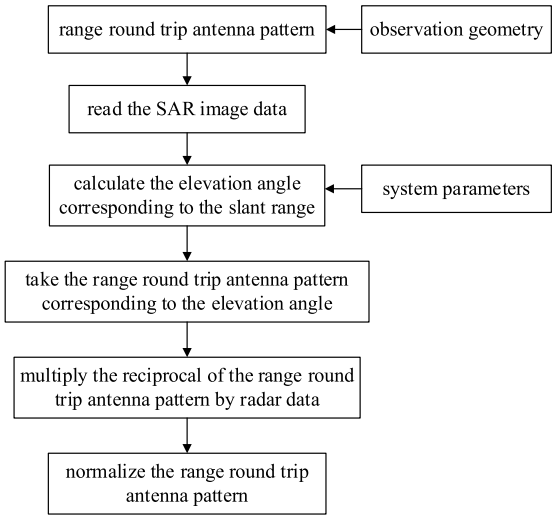

Fig. 8. Flowchart of the antenna pattern correction.

2) Read the bistatic SAR image data.
3) Calculate the elevation angle range of the bistatic SAR range round trip antenna pattern corresponding to the slant range considering the system parameters and the imaging geometry.
4) Obtain the range round trip antenna pattern corresponding to the elevation angle.
5) Multiply the reciprocal of the range round trip antenna pattern by radar data for normalization.

In this section, bistatic SAR imaging simulation experiments are conducted to verify the effectiveness of this correction method by comparing the point target energy before and after correction. The bistatic SAR imaging system parameters are shown in Table I, and the imaging algorithm is the range–Doppler (RD) algorithm. It is assumed that the signal-to-noise ratio (SNR) is 25 dB and the noise signal is White Gaussian Noise. Moreover, the swath width is 1800 m, and nine point targets are selected in the range with an interval of 200 m, i.e., 100, 300, 500, 700, 900, 1100, 1300, 1500, and 1700 m.

In the following simulation experiments, the transmitting and receiving antenna patterns are used in the bistatic SAR echo simulation, and the simulation images are corrected based

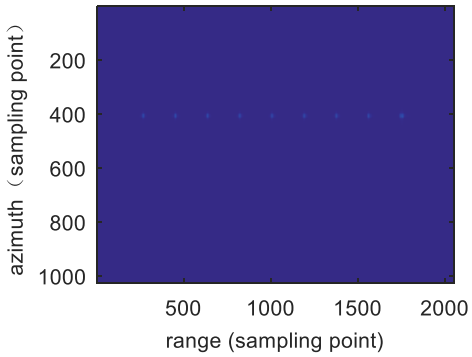

Fig. 9. Image result before pattern correction.

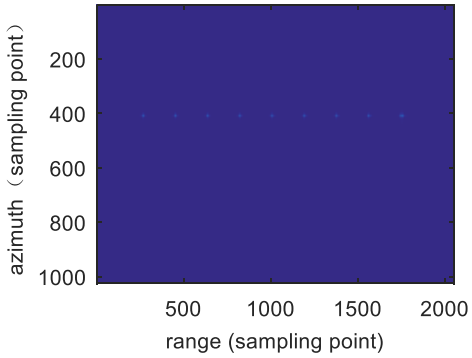

Fig. 10. Image result after pattern correction.

TABLE III
POINT TARGET ENERGY BEFORE AND AFTER CORRECTION

Range (m)	Before correction (dB)	After correction (dB)
100	16.0682	17.2622
300	16.5275	17.4092
500	16.8611	17.3512
700	17.1605	17.3129
900	17.2515	17.2531
1100	17.1366	17.2342
1300	16.9119	17.3104
1500	16.2583	17.3160
1700	16.0093	17.1829

on this antenna pattern correction method. The image results before and after correction are shown in Figs. 9 and 10, and the points target energy are shown in Table III. The uncorrected image shows a high brightness of the point target in the center and a decreasing illumination to the borders of the image in the range direction. This is caused by the antenna pattern spanning over range. In addition, the maximum difference between each point target energy is approximately 1 dB, which indicates that the brightness of each point target is different in the image. After correction, the same acquisition after antenna pattern correction with the characteristics of the antenna being eliminated, the point target energy in different ranges is basically the same, and the maximum difference is approximately 0.2 dB, which can meet the basic radiometric correction requirements. Therefore, the antenna pattern correction method is effective.

V. CONCLUSION

In this letter, the comodulation effect introduced by transmitting and receiving antennas is analyzed and also pointed out that the range variation of the bistatic angle in the swath will affect the range round trip antenna pattern. They are, therefore, helpful for designing measurement equipment and methods to obtain the round trip antenna pattern. Moreover, the variations in the bistatic angle and the beam pointing error for the range round trip antenna patterns are analyzed to ensure that the radiometric calibration accuracy is sufficient. Theoretical analysis and simulation results also demonstrate that the comodulation effect of correction method based on precise antenna models is validated.

REFERENCES

[1] A. Freeman, "SAR calibration: An overview," *IEEE Trans. Geosci. Remote Sens.*, vol. 30, no. 6, pp. 1107–1121, Nov. 1992.
[2] M. C. Dobson, F. T. Ulaby, D. R. Brunfeldt, and D. N. Held, "External calibration of SIR-B imagery with area-extended and point targets," *IEEE Trans. Geosci. Remote Sens.*, vols. GE–24, no. 4, pp. 453–461, Jul. 1986.
[3] M. Shimada and A. Freeman, "A technique for measurement of space-borne SAR antenna patterns using distributed targets," *IEEE Trans. Geosci. Remote Sens.*, vol. 33, no. 1, pp. 100–114, Jan. 1995.
[4] C. J. Bradley *et al.*, "An investigation of bistatic calibration objects," *IEEE Trans. Geosci. Remote Sens.*, vol. 43, no. 10, pp. 2177–2184, Oct. 2005.
[5] Q. Zheng, Y. Wang, J. Hong, and A. Wang, "Feasibility, design, and deployment requirements of TCR for bistatic SAR radiometric calibration," *Remote Sens.*, vol. 10, no. 10, p. 1610, Oct. 2018.
[6] A. A. Thompson, D. Racine, and A. P. Luscombe, "RADARSAT-2 antenna calibration using ground receivers/transmitters," in *Proc. IEEE Int. Geosci. Remote Sens. Symp.*, vol. 3, Jun. 2002, pp. 1465–1467.
[7] P. Seifert, H. Lentz, M. Zink, and F. Heel, "Ground-based measurements of inflight antenna patterns for imaging radar systems," *IEEE Trans. Geosci. Remote Sens.*, vol. 30, no. 6, pp. 1131–1136, Nov. 1992.
[8] W.-Q. Wang, "Inflight antenna pattern measurement for bistatic synthetic aperture radar systems," *IEEE Antennas Wireless Propag. Lett.*, vol. 6, pp. 432–435, 2007.
[9] M. Bachmann, M. Schwerdt, and B. Brautigam, "TerraSAR-X antenna calibration and monitoring based on a precise antenna model," *IEEE Trans. Geosci. Remote Sens.*, vol. 48, no. 2, pp. 690–701, Feb. 2010.
[10] J.-L. Bueso-Bello, M. Martone, P. Prats-Iraola, and B. Bruutigam, "First characterization and performance evaluation of bistatic TanDEM-X experimental products," *IEEE J. Sel. Topics Appl. Earth Observ. Remote Sens.*, vol. 9, no. 3, pp. 1058–1071, Mar. 2016.
[11] A. M. Horne and G. Yates, "Bistatic synthetic aperture radar," in *Proc. IEEE Radar Conf.*, Oct. 2002, pp. 6–10.
[12] B. Zhao, X. Bai, F. Zhou, Z. Zhang, and Z. Bao, "Analysis of the azimuth resolution of bistatic SAR," in *Proc. Int. Conf. Radar*, Sep. 2013, pp. 407–411.
[13] Q. Zheng, "Research on key technologies of bistatic radiometric calibration for distributed SAR satellites," (in Chinese), M.S. thesis, Dept. Sci. Eng., Inst. Electron., Chin. Acad. Sci., Beijing, China, 2019.
[14] T. A. Milligan, *Modern Antenna Design*, 2nd ed. Piscataway, NJ, USA: IEEE Press, 2005.
[15] J. Ender, "A step to bistatic SAR processing," in *Proc. EUSAR*, Ulm, Germany, May 2004, pp. 359–363.
[16] W. Pu, J. Wu, Y. Huang, J. Yang, and H. Yang, "Fast factorized backprojection imaging algorithm integrated with motion trajectory estimation for bistatic forward-looking SAR," *IEEE J. Sel. Topics Appl. Earth Observ. Remote Sens.*, vol. 12, no. 10, pp. 3949–3965, Oct. 2019.
[17] G. Krieger *et al.*, "TanDEM-X: A satellite formation for high-resolution SAR interferometry," *IEEE Trans. Geosci. Remote Sens.*, vol. 45, no. 11, pp. 3317–3341, Nov. 2007.
[18] P. Dubois-Fernandez *et al.*, "ONERA-DLR bistatic SAR campaign: Planning, data acquisition, and first analysis of bistatic scattering behaviour of natural and urban targets," *IEE Proc. Radar, Sonar Navigat.*, vol. 153, no. 3, p. 214, 2006.
[19] M. Schwerdt, B. Brautigam, M. Bachmann, B. Doring, D. Schrank, and J. H. Gonzalez, "Final TerraSAR-X calibration results based on novel efficient methods," *IEEE Trans. Geosci. Remote Sens.*, vol. 48, no. 2, pp. 677–689, Feb. 2010.